

Rossby Wave Instability with Self-Gravity

R.V.E. Lovelace¹ & R.G. Hohlfield^{2,3}

¹*Department of Astronomy, Cornell University, Ithaca, NY 14853; email: lovelace@astro.cornell.edu*

²*Center for Computational Science, Boston University, 3 Cummington Street, Boston MA 02215;*

³*Wavelet Technologies, Inc. 664 Pike Ave., Attleboro MA 02703; RHohlfield@wavelettech.com*

24 February 2022

ABSTRACT

The Rossby wave instability (RWI) in non-self-gravitating discs can be triggered by a bump at a radius r_0 in the disc surface mass-density (which is proportional to the inverse potential vorticity). It gives rise to a growing non-axisymmetric perturbation $[\propto \exp(im\phi), m = 1, 2..]$ in the vicinity of r_0 consisting of *anticyclonic* vortices which may facilitate planetesimal growth in protoplanetary discs. Here, we analyze a continuum of thin disc models ranging from self-gravitating to non-selfgravitating. The key quantities determining the stability/instability are: (1) the parameters of the bump (or depression) in the disc surface density, (2) the Toomre Q parameter of the disc (a non-self-gravitating disc has $Q \gg 1$), and (3) the dimensionless azimuthal wavenumber of the perturbation $\bar{k}_\phi = mQh/r_0$, where h is the half-thickness of the disc. For discs stable to axisymmetric perturbations ($Q > 1$), the self-gravity has a significant role for $\bar{k}_\phi < \pi/2$ or $m < (\pi/2)(r_0/h)Q^{-1}$; instability may occur for a depression or groove in the surface density if $Q \lesssim 2$. For $\bar{k}_\phi > \pi/2$ the self-gravity is not important, and instability may occur at a bump in the surface density. Thus, for all mode numbers $m \geq 1$, the self-gravity is unimportant for $Q > (\pi/2)(r_0/h)$. We suggest that the self-gravity be included in simulations for cases where $Q < (r_0/h)$.

Key words: accretion, accretion discs — instabilities — hydrodynamics — waves — spiral galaxies

1 INTRODUCTION

The theory of the Rossby wave instability (RWI) was developed by Lovelace et al. (1999) and Li et al. (2000) for thin accretion discs with negligible self-gravity and earlier by Lovelace & Hohlfield (1978) for thin disc galaxies where the self-gravity may or may not be important. In the first case the instability can occur if there is a bump as a function of radius in the inverse potential vorticity $F(r) \propto \Sigma\Omega[(\nabla \times \mathbf{u}) \cdot \hat{\mathbf{z}}]^{-1}$ at some radius r_0 , where Σ is the surface mass density, Ω the angular velocity, and \mathbf{u} the flow velocity of the disc. Such a bump could arise at the radial boundary of the “dead zone” (Varnière & Tagger 2006; Lyra et al. 2009; Crespe et al. 2011). This zone can arise from the suppression of the magnetorotational instability by low ionization inside the disc (Gammie 1996). In turn, the bump in $F(r)$ can give rise to the exponential growth of non-axisymmetric perturbations in the vicinity of r_0 consisting of *anticyclonic* vortices. Such vortices can act to concentrate dust grains in their centres and thereby accelerate the formation of macroscopic planetesimals (Barge & Sommeria 1995; Tanga et al. 1996; Bracco et al. 1999; Godon &

Livio 2000; Johansen et al. 2004; Heng & Kenyon 2010). Two-dimensional hydrodynamic simulations of the RWI instability in discs were done by Li et al. (2001) and recently in three dimensions (e.g., Meheut et al. 2010, 2012a). The theory of the instability in three dimensions has been studied by Meheut et al. (2012b) and Lin (2012). The instability is also predicted to occur in strongly non-Keplerian discs with regions where $d\Omega/dr > 0$ which exist around rotating magnetized stars (Lovelace et al. 2009). In the RWI the wave is radially trapped within the disc which is different from the Papaloizou and Pringle (1984; 1985) instability where the wave is trapped between the inner and outer radii of a disc or torus. The RWI has an important role in the accretion-ejection instability of discs proposed by Tagger and collaborators (e.g., Tagger & Varnière 2006; Tagger & Melia 2006; Tagger & Pellat 1999).

The RWI in disc galaxies consisting mainly of stars has been studied using N -body simulations (Sellwood & Kahn 1991; and Sellwood 2012). When the self-gravity of the disc is important, instability occurs at radii where $F(r)$ has a minimum, that is, a groove (Lovelace & Hohlfield 1978; Sell-

wood & Kahn 1991). We do not consider the instability of self-gravitating gas discs for conditions where the gas cooling is important (Gammie 2001).

Saturation of the exponential growth of the instability is predicted to occur when the time-scale for a fluid particle to orbit the center of a vortex is comparable to the wave's growth time-scale (Lovelace et al. 2009). Simulations by Meheut et al. 2012c) support this conclusion.

Section 2 develops the theory, applies it to radially localized perturbations, and considers axisymmetric and nonaxisymmetric modes. Section 3 gives sample results for cases where self-gravity is important and where it is negligible, and Sec. 4 gives a numerical example relevant to forming protostar. Conclusions are given in Sec. 4.

2 THEORY

We consider the stability of a thin self-gravitating disc of equilibrium surface mass density $\Sigma(r)$ with a (r, ϕ, z) coordinate system. The equilibrium has the flow velocity $\mathbf{u} = u_\phi(r)\hat{\phi} = r\Omega(r)\hat{\phi}$. That is, the accretion velocity u_r and the vertical velocity u_z are assumed negligible compared with u_ϕ . The equilibrium flow satisfies $-\Sigma r\Omega^2 = -dP/dr - \Sigma\nabla\Phi$, where P the vertically integrated pressure and Φ the gravitational potential. This potential is given by $\nabla^2\Phi = 4\pi G\Sigma\delta(z)$, where G is the gravitational constant.

The perturbed quantities are: the density, $\tilde{\Sigma} = \Sigma + \delta\Sigma(r, \phi, t)$; the pressure is $\tilde{P} = P + \delta P(r, \phi, t)$; the flow velocity is $\tilde{\mathbf{u}} = \mathbf{u} + \delta\mathbf{u}(r, \phi, t)$ with $\delta\mathbf{u} = (\delta u_r, \delta u_\phi, 0)$. The equations for the perturbed flow are

$$\frac{D\tilde{\Sigma}}{Dt} + \tilde{\Sigma} \nabla \cdot \tilde{\mathbf{u}} = 0, \quad (1a)$$

$$\frac{D\tilde{\mathbf{u}}}{Dt} = -\frac{1}{\tilde{\Sigma}}\nabla\tilde{P} - \nabla\Phi, \quad (1b)$$

$$\frac{D\tilde{S}}{Dt} = 0, \quad (1c)$$

where $D/Dt \equiv \partial/\partial t + \tilde{\mathbf{u}} \cdot \nabla$, and where $S \equiv \tilde{P}/(\tilde{\Sigma})^\gamma$ is the entropy of the disc matter.

We consider perturbations $\sim f(r)\exp(im\phi - i\omega t)$, where $m = 0, 1, 2, \dots$ is the azimuthal mode number and ω the angular frequency. For free perturbations $\omega = \omega_r + i\omega_i$ and for the growing modes of interest $\omega_i > 0$. From equation (1a), we have

$$i\Delta\omega \delta\Sigma = \nabla \cdot (\Sigma \delta\mathbf{u}), \quad (2)$$

where

$$\Delta\omega(r) \equiv \omega - m\Omega(r),$$

and $\Omega = u_\phi/r$.

From equation (1b) we have

$$i\Delta\omega\delta u_r + 2\Omega\delta u_\phi = \frac{1}{\tilde{\Sigma}}\frac{\partial\delta P}{\partial r} - \frac{\delta\Sigma}{\tilde{\Sigma}^2}\frac{dP}{dr} + \nabla\delta\Phi, \quad (3a)$$

$$i\Delta\omega\delta u_\phi - \frac{\Omega_r^2}{2\Omega}\delta u_r = ik_\phi\frac{\delta P}{\Sigma} + ik_\phi\delta\Phi \quad (3b)$$

Here, $\Omega_r \equiv [r^{-3}d(r^4\Omega^2)/dr]^{1/2}$ is the radial epicyclic frequency, and $k_\phi \equiv m/r$ is the azimuthal wavenumber. For an approximately Keplerian disc, $\Omega_r \approx \Omega$.

From equation (1c) and (1d), we have

$$\delta P = c_s^2\delta\Sigma - \frac{i\Sigma c_s^2}{\Delta\omega L_S}\delta u_r.$$

Here, $c_s = (dP/d\Sigma)_S^{1/2}$ is the effective sound speed in the disc and $L_S^{-1} \equiv \gamma^{-1}d\ln(S)/dr$ with L_S the length-scale of the entropy $S = P/\Sigma^\gamma$ variation in the disc. To simplify the subsequent calculations we consider the homentropic case where $L_S \rightarrow \infty$.

The perturbation of the gravitational potential is given by

$$\nabla^2\delta\Phi = 4\pi G\delta\Sigma\delta(z). \quad (4)$$

Equations (3) can be solved to give

$$\Sigma\delta u_r = iF \left[\frac{\Delta\omega}{\Omega} \frac{\partial\delta\Psi}{\partial r} - 2k_\phi\delta\Psi \right], \quad (5a)$$

$$\Sigma\delta u_\phi = F \left[\frac{\Omega_r^2}{2\Omega^2} \frac{\partial\delta\Psi}{\partial r} - k_\phi \frac{\Delta\omega}{\Omega} \delta\Psi \right], \quad (5b)$$

where

$$\delta\Psi \equiv c_s^2 \frac{\delta\Sigma}{\Sigma} + \delta\Phi, \quad (5c)$$

is an effective potential and

$$F \equiv \frac{\Sigma\Omega}{\Omega_r^2 - (\Delta\omega)^2}, \quad (5d)$$

is the function identified by Lovelace and Hohlfield (1978).

Substituting equations (5) into (2) we obtain

$$\delta\Sigma = \frac{1}{r} \frac{\partial}{\partial r} \left(\frac{rF}{\Omega} \frac{\partial\delta\Psi}{\partial r} \right) - k_\phi^2 \frac{F}{\Omega} \delta\Psi - \frac{2k_\phi}{\Delta\omega} \frac{dF}{dr} \delta\Psi, \quad (6)$$

2.1 Radially Localized Modes

Here we consider radially localized modes in the sense that perturbation extends over a radial region Δr with $(\Delta r)^2 \ll r^2$ centred at r_0 . With this in mind we rewrite equation (6) as

$$\begin{aligned} (\Omega_r^2 - \Delta\omega^2) \frac{\delta\Sigma}{\Sigma} &= \frac{d^2\delta\Psi}{dr^2} - k_\phi^2\delta\Psi \\ &+ \frac{d\ln\tilde{F}}{dr} \frac{d\delta\Psi}{dr} - \frac{2k_\phi\Omega}{\Delta\omega} \frac{d\ln F}{dr} \delta\Psi, \end{aligned} \quad (7)$$

where $\tilde{F} \equiv rF/\Omega$.

We let

$$(\delta\Sigma_{k_r}, \delta\Psi_{k_r}) = \int \frac{dr}{2\pi} (\delta\Sigma, \delta\Psi) \exp[-ik_r(r - r_0)],$$

where k_r is the radial wavenumber of the perturbation. The radial Fourier transform of equation (7) gives

$$\begin{aligned} (\Omega_r^2 - \Delta\omega^2) \frac{\delta\Sigma_{k_r}}{\Sigma} &= -\mathbf{k}^2\delta\Psi_k \\ &+ \left(\frac{d\ln\tilde{F}}{dr} \frac{d\delta\Psi}{dr} - \frac{2k_\phi\Omega}{\Delta\omega} \frac{d\ln F}{dr} \delta\Psi \right)_{k_r}. \end{aligned} \quad (8)$$

Here, we have neglected the radial variation of Σ and Ω_r , and that of $\Delta\omega^2$ in comparison with Ω_r^2 . Also, $\mathbf{k} = k_r\hat{r} + k_\phi\hat{\phi}$ and $(\cdot)_{k_r}$ denotes the Fourier transform.

Assuming $|k_r| \sim (\Delta r)^{-1} \gg r_0$, the WKBJ solution of

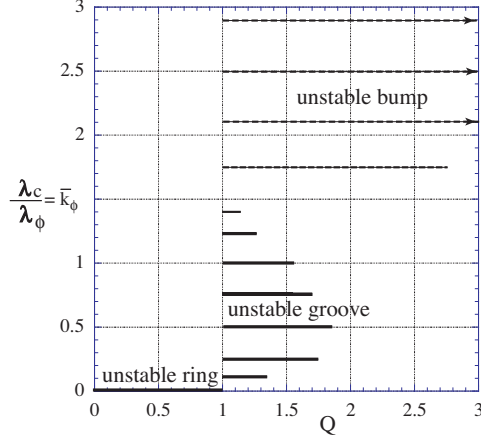


Figure 1. The horizontal lines mark out the regions of ‘bump’ and ‘groove’ instability in a self-gravitating disc for $m = 3$ and the ring instability for $m = 0$. Here, $\lambda_c = 2\pi/k_c$ and $\lambda_\phi = 2\pi/k_\phi$. For the $Q > 1$ part of the figure we have used equations (12) and (15) with $\Delta F = 0.2$ for the bump and $\Delta F = -0.2$ for the groove, $\Delta x = 0.04$, and $q = 3/2$.

equation (4) gives $\delta\Phi_{k_r} = -2\pi G\delta\Sigma_{k_r}/|\mathbf{k}|$. Therefore, from equation (5c) we obtain

$$\delta\Psi_{k_r} = \left(1 - \frac{2k_c}{|\mathbf{k}|}\right) c_s^2 \frac{\delta\Sigma_{k_r}}{\Sigma}, \quad (9a)$$

where

$$k_c \equiv \frac{\pi G \Sigma}{c_s^2} \quad (9b)$$

is a characteristic wavenumber.

2.1.1 Axisymmetric Modes

For axisymmetric perturbations ($k_\phi = 0 = m$) of smooth disc (where the term $\propto d\ln\tilde{F}/dr$ can be neglected in equation (8)), equations (8) and (9a) give

$$\omega^2 = \Omega_r^2 + k_r^2 c_s^2 - 2k_c |k_r|, \quad (10)$$

(Safranov 1960; Toomre 1964). The minimum of $[\omega(k_r)]^2$ occurs at $k_r = k_c$ where $\omega^2 = \Omega_r^2 - k_c^2 c_s^2$. Therefore, if we define $k_{c*} \equiv \Omega_r/c_s$, then for $k_c < k_{c*}$ the minimum of ω^2 is positive and the axisymmetric perturbations are stable. Conversely for $k_c > k_{c*}$ the perturbations are unstable. With

$$Q \equiv \frac{k_{c*}}{k_c} = \frac{\Omega_r c_s}{\pi G \Sigma}, \quad (11)$$

the axisymmetric perturbations are stable (unstable) for $Q > 1$ ($Q < 1$) (Toomre 1964). The minimum value of the squared frequency is $\omega(k_r)^2 = (k_{c*} c_s)^2 (1 - Q^{-2})$. Figure 1 shows the unstable region for a ring, $Q < 1$.

2.1.2 Non-Axisymmetric Modes

For the non-axisymmetric perturbations ($m = 1, 2, \dots$, $k_\phi = m/r$) we assume that $(\Delta\omega)^2 \ll \Omega_r^2$ in equation (8). Multiplying equation (8) by $(1 - 2k_c/|\mathbf{k}|)$ and doing the inverse Fourier transform gives

$$\delta\Psi(x) = \frac{2}{\pi} \int_{-\infty}^{\infty} dx' K(x-x') \frac{\Omega}{\Delta\omega(x')} \frac{d\ln F}{dx'} \delta\Psi(x'). \quad (12a)$$

This represents an integral equation for $\delta\Psi(x)$. The term in equation (8) proportional to $d\ln\tilde{F}/dr$ has been dropped. It is negligible compared with the term involving $d\ln F/dr$ because $|m\Omega/\Delta\omega| \gg 1$ for the considered modes. The kernel is

$$K(x) = \frac{2}{\pi} \int_0^\infty dy \frac{\cos(mxy) \left(\frac{2}{\bar{k}_\phi \sqrt{1+y^2}} - 1 \right)}{\left(1 + y^2 + \frac{Q^2}{\bar{k}_\phi^2} - \frac{2\sqrt{1+y^2}}{\bar{k}_\phi} \right)}. \quad (12b)$$

Here, $x \equiv (r - r_0)/r_0$ with $x^2 \ll 1$, $\Omega = \Omega(r_0)$, Q is given in equation (11), and $\bar{k}_\phi \equiv k_\phi/k_c$.

The half-thickness of the disc h is c_s/Ω_r so that

$$\frac{\bar{k}_\phi}{mQ} = \frac{h}{r}, \quad (13)$$

where we assume $(h/r)^2 \ll 1$. Note that $\lambda_c = 2\pi/k_c = 2\pi hQ$. The Toomre (1964) characteristic wavelength is defined as $\lambda_* = 4\pi G\Sigma/\Omega_r^2 = 4h/Q$. Thus $\lambda_c/\lambda_* = \pi Q^2/2$.

In parallel with equations (12) note that

$$c_s^2 \frac{\delta\Sigma(x)}{\Sigma} = \frac{2}{\pi} \int_{-\infty}^{\infty} dx' G(x-x') \frac{\Omega}{\Delta\omega(x')} \frac{d\ln F}{dx'} \delta\Psi(x'). \quad (14a)$$

Here,

$$G(x) = -\frac{2}{\pi} \int_0^\infty dy \frac{\cos(mxy)}{\left(1 + y^2 + \frac{Q^2}{\bar{k}_\phi^2} - \frac{2\sqrt{1+y^2}}{\bar{k}_\phi} \right)}, \quad (14b)$$

is a second kernel.

We solve equation (12) for the case where $\ln[F(x)]$ has a square bump or groove. That is,

$$\ln[F(x)] = \Delta F H(x + \Delta x/2) H(\Delta x/2 - x), \quad (15)$$

where H is the Heaviside step function (+1 for positive argument and zero for a negative argument), and Δx is the fractional radial width of the bump ($\Delta F > 0$) or groove ($\Delta F < 0$). This distribution of $\ln F$ is known to be useful for analytic calculations of the non-axisymmetric instability of discs (Sellwood & Kahn 1991; Umurhan 2010).

Substituting equation (15) into (12) gives

$$\delta\Psi_- = \frac{2}{\pi} K_0 \frac{\Omega \Delta F}{\Delta\omega_-} \delta\Psi_- - \frac{2}{\pi} K_{\Delta x} \frac{\Omega \Delta F}{\Delta\omega_+} \delta\Psi_+, \quad (16a)$$

$$\delta\Psi_+ = \frac{2}{\pi} K_{\Delta x} \frac{\Omega \Delta F}{\Delta\omega_-} \delta\Psi_- - \frac{2}{\pi} K_0 \frac{\Omega \Delta F}{\Delta\omega_+} \delta\Psi_+, \quad (16b)$$

where $K_0 = K(0)$, $K_{\Delta x} = K(\Delta x)$ and $\Delta\omega_\pm = \omega - m\Omega[r_0(1 \pm \Delta x/2)] \approx \omega - m\Omega \pm qm\Delta x\Omega/2$ for the $q \equiv -d\ln\Omega/d\ln r$ with $q = 3/2$ for a Keplerian disc. Equations (16) give a quadratic in ω which for the assumed symmetry of the bump or groove about $x = 0$ gives either $(\omega - m\Omega)^2 > 0$ - stable motion - or $(\omega - m\Omega)^2 < 0$ - unstable motion.

Evidently an arbitrary $\ln[F(r)]$ can be approximated by a staircase-like function with the result that equation (12) leads to an $n \times n$ matrix equation in place of equation (16) with n the number of steps.

3 SAMPLE RESULTS

The main parameters of importance for instability are: (1) The parameters of the bump or groove (ΔF and Δx). (2)

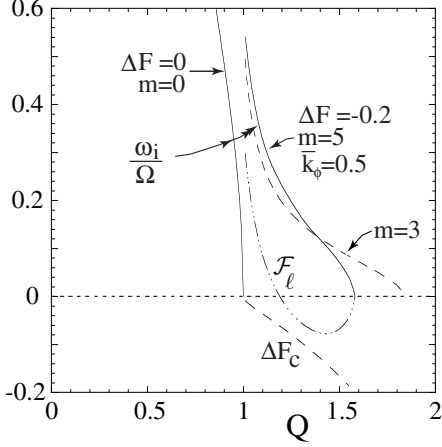


Figure 2. Growth rates of axisymmetric perturbations ($m = 0$) for $Q < 1$ and non-axisymmetric perturbations ($m = 3, 5$) for $Q > 1$ for a groove ($\Delta F < 0$) in the $F(r)$ profile, $\bar{k}_\phi = \lambda_c/\lambda_\phi = 0.5$, and $q = 3/2$. Here, ΔF_c is the threshold value of the depth of the groove ΔF needed for instability. Also, \mathcal{F}_ℓ is proportional to the radial angular momentum flux across the centre of the groove as discussed in the text. For the $Q > 1$ part of this figure we have used equations (12) and (15) with $\Delta F = -0.2$ for the groove and $\Delta x = 0.04$.

The parameters of the disc Q and of the perturbation m and $\bar{k}_\phi = k_\phi/k_c$. Figure 1 gives a qualitative picture of the regions of bump, groove, and ring instability in a disc as a function of Q and $\bar{k}_\phi = k_\phi/k_c$. The needed kernel in equation (12b) is accurately evaluated numerically using a 4000 point integration. (Our attempt to analytically integrate (12b) was thwarted by the required branch cuts at the points $y = \pm i$.) The transition from groove to bump instability occurs when $K(0)$ goes through zero as a function of \bar{k}_ϕ , with $K(0) > 0$ for small \bar{k}_ϕ . We find that this occurs at $\bar{k}_\phi \approx 1.55$. This agrees with the conclusion of Lovelace and Hohlfield (1978) that the transition is at $\bar{k}_\phi = \pi/2 \approx 1.57$.

Figure 2 shows the growth rates as a function of Q for the ring mode ($m = 0$ and $Q < 1$) and the groove mode ($m = 3, 5$, $Q > 1$, and $\bar{k}_\phi = 0.5$). Also shown in the figure is ΔF_c which is the minimum groove depth needed for instability. Further, \mathcal{F}_ℓ is proportional to the radial angular momentum flux across the $x = 0$ surface. Specifically, $\mathcal{F}_\ell \propto r \int d\phi \Re(r^2 \Omega \delta \Sigma^* \delta u_r + \Sigma r \delta u_\phi^* \delta u_r)$, where \Re denotes the real part.

Generally, for both unstable grooves and bumps the growth rate increases as $|\Delta F|$ increases above a threshold value. Also, the growth rate decreases as the width of the groove or bump Δx increases. This supports the interpretation of Umurhan (2010) that the instability of a bump arises from interaction “edge waves” on the surfaces where F changes rapidly.

Unstable grooves: Figure 3 shows the density perturbation $\delta \Sigma(r, \phi)$ and the arrows represent the flow perturbation $(\delta u_r, \delta u_\phi)$ for an unstable groove with $\Delta F = -0.2$, and $Q = 1.3$, $m = 3$, and $\bar{k}_\phi = 0.5$. Notice that the anticyclonic motion of the vortex about the *minimum* of the density perturbation.

Unstable bumps: Figure 4 shows the density perturbation $\delta \Sigma(r, \phi)$ and the arrows represent the flow perturbation

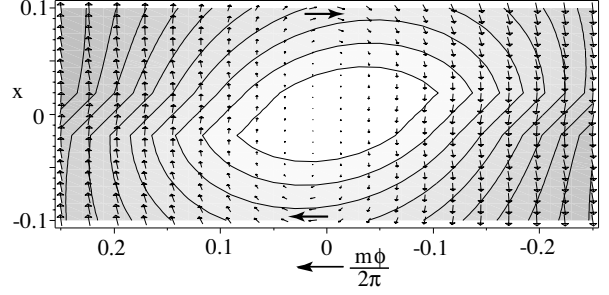


Figure 3. The background gray-scale (white=low, dark=high) and the contours represent the density perturbation $\delta \Sigma(r, \phi)$, and the arrows represent the flow perturbation $(\delta u_r, \delta u_\phi)$ for the case of an unstable groove, $\Delta F = -0.2$, and $Q = 1.3$, $m = 3$, $\bar{k}_\phi = 0.5$, and $q = 3/2$. The growth rate is $\omega_i/\Omega = 0.152$. The larger arrows near the top and bottom of the figure have been put in to make clear the direction of the circulation which is anticyclonic. In this case this circulation is around a minimum of the density perturbation.

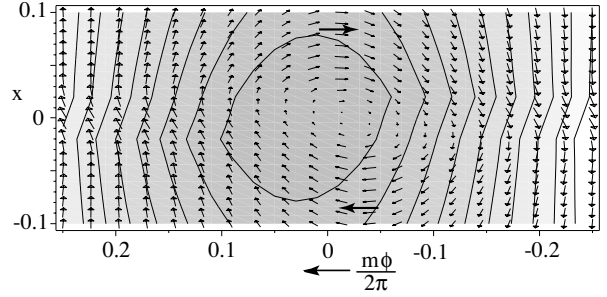


Figure 4. The background gray-scale (white=low, dark=high) and the contours represent the density perturbation $\delta \Sigma(r, \phi)$, and the arrows represent the flow perturbation $(\delta u_r, \delta u_\phi)$ for the case of an unstable bump, $\Delta F = 0.2$, and $Q = 1.3$, $m = 3$, $\bar{k}_\phi = 2$, and $q = 3/2$. The growth rate is $\omega_i/\Omega = 0.0844$. The larger arrows near the top and bottom of the figure have been put in to make clear the direction of the circulation which is anticyclonic. In this case this circulation is approximately around a maximum of the density perturbation.

tion $(\delta u_r, \delta u_\phi)$ for an unstable bump with $\Delta F = 0.2$, and $Q = 1.3$, $m = 3$, and $\bar{k}_\phi = 2$. Notice that the center of the anticyclonic motion of the vortex is offset by a small angle from the *maximum* of the density perturbation. The angular momentum flux across $x = 0$ is found to be always outward for unstable bumps.

Figure 5 shows a further case of an unstable bump with $\Delta F = 0.2$, and $Q = 2$, $m = 3$, and $\bar{k}_\phi = 2$. The center of the anticyclonic motion of the vortex is again offset by a small angle from the *maximum* of the density perturbation.

4 NUMERICAL EXAMPLES

We first consider an accretion disc around a solar mass star with accretion rate $\dot{M} = 10^{-8} M_\odot \text{yr}^{-1}$. For an α -viscosity disc with $\alpha = 5 \times 10^{-3}$, the surface mass density is $\Sigma = 89.3 \text{ g cm}^{-2}$ at $r = 10 \text{ AU}$ assuming the half-thickness of the

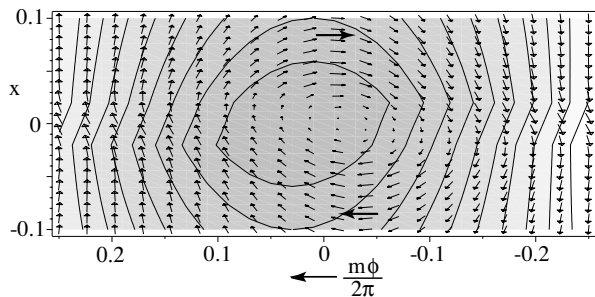


Figure 5. The background gray-scale (white=low, dark=high) and the contours represent the density perturbation $\delta\Sigma(r, \phi)$, and the arrows represent the flow perturbation $(\delta u_r, \delta u_\phi)$ for the case of an unstable bump, $\Delta F = 0.2$, and $Q = 2$, $m = 3$, $\bar{k}_\phi = 2$, and $q = 3/2$. The growth rate is $\omega_i/\Omega = 0.0661$. The larger arrows near the top and bottom of the figure have been put in to make clear the direction of the circulation which is anticyclonic. In this case this circulation is approximately around a maximum of the density perturbation.

disc is $h = 0.04r$ or $c_s/v_K = 0.04$, where c_s is the isothermal sound speed in the disc and $v_K = 9.4 \text{ km s}^{-1}$ is the Keplerian velocity. We have used $\dot{M} = 2\pi r \Sigma u_r$ with $u_r = \alpha c_s^2/v_K$. For comparison, the surface mass-density of a Jupiter mass spread over a radial extent $2h$ at 10AU is about 170 g cm^{-2} . From equations (9b) and (10), $k_c = 1.97/r$ and $Q = 12.7$. For fixed c_s/v_K , notice that $Q \propto \dot{M}/\alpha$. In equation (13) we have $\bar{k}_\phi = 0.04mQ = 0.508m$. For $\bar{k}_\phi < \pi/2$ or $m \leq 3$ there is no instability because $Q \gg 1$. We have a bump instability for $m > 3$. Clearly, all of the modes $m \geq 1$ are in the bump regime if $Q > \pi r/(2h)$. The mass of the disc is relatively small, $\sim \pi r^2 \Sigma/M_\odot = (c_s/v_K)/Q = 0.0031$, so that it is approximately Keplerian.

As a second case, consider a larger accretion rate $\dot{M} = 3 \times 10^{-8} M_\odot \text{ yr}^{-1}$ and a smaller viscosity $\alpha = 0.002$ but with the other quantities (r, c_s) the same as above. Then we find that $Q = 1.69$ and $\bar{k}_\phi = 0.0676m$. For $\bar{k}_\phi < \pi/2$ or $m \leq 23$ there can be a groove instability because Q is not much larger than unity (see Fig. 1). At the same time we expect the bump instability for $m > 23$ to be unimportant because the azimuthal wavelengths are comparable to the disc half-thickness.

5 CONCLUSIONS

We have analyzed the Rossby wave instability in a continuum of thin disc models ranging from self-gravitating to non-selfgravitating. The important quantities determining the stability/instability are: (1) the parameters of the bump (or depression) in the inverse potential vorticity $F(r)$ at r_0 , (2) the Toomre Q parameter of the disc, and (3) the dimensionless azimuthal wavenumber of the perturbation $\bar{k}_\phi = mQh/r_0$, where h is the half-thickness of the disc and $m = 1, 2, \dots$ is the azimuthal mode number. For $\bar{k}_\phi < \pi/2$ and $Q \lesssim 2$ instability may occur for the case of a groove in the surface-density. In this case the centres of the anticyclonic vortices have reduced density. For $\bar{k}_\phi < \pi/2$ $Q > 2$, both bumps and grooves are stable. For $\bar{k}_\phi > \pi/2$, the bumps may be unstable and the centres of the anticy-

clonic vortices have density enhancements. The growth rates for both the groove and bump instability are $\lesssim 10\%$ of the orbital angular frequency for bumps fractional amplitude $\lesssim 20\%$.

For fixed radius r_0 and sound speed c_s , the regime of instability - groove or bump - is set by the Q value which is proportional to \dot{M}/α with α the dimensionless viscosity. For $Q \lesssim 2$ and $m < (\pi/2)(r_0/h)Q^{-1}$ the groove instability may occur. On the other hand for $Q \gg 1$ and $m > (\pi/2)(r_0/h)Q^{-1}$ the bump instability may occur. The estimates of Sec. 4 indicate that the two regimes are not widely separated in terms of \dot{M} and α . For this reason we suggest that simulations of Rossby vortices include the self-gravity for cases where $Q < r_0/h$.

ACKNOWLEDGEMENTS

We thank the referee for helpful criticism. RVEL was supported in part by NASA grant NNX11AF33G.

REFERENCES

- Barge, P., & Sommeria, J. 1995, A&A, 295, L1
- Bracco, A., Chavanis, P.H., Provenzale, A., & Spiegel, E.A. 1999, Phys. Fluids, 11, 2280
- Crespe E., Gonzalez J.-F., & Arena S. E., 2011, in SF2A-2011: Proceedings of the Annual meeting of the French Society of Astronomy and Astrophysics, G. Alecian, K. Belkacem, R. Samadi, & D. Valls-Gabaud, ed., pp. 469473
- Gammie, C.F. 1996, ApJ, 457, 355
- Gammie, C.F. 2001, ApJ, 553, 174
- Godon, P., & Livio, M. 2000, ApJ, 537, 396
- Heng, K., & Kenyon, S.J. 2010, MNRAS, 408, 1476
- Johanssen, A., Andersen, A.C., & Brandenburg, A. 2004, A&A, 417, 361
- Li, H., Finn, J.M., Lovelace, R.V.E., & Colgate, S.A. 2000, ApJ, 533, 1023
- Li, H., Colgate, S.A., Wendroff, B., & Liska, R. 2001, ApJ, 551, 874
- Lin, M.-K., 2012, ApJ, 754, 21
- Lovelace, R.V.E., & Hohlfield, R.G. 1978, ApJ, 221, 51
- Lovelace, R.V.E., Li, H., Colgate, S.A., & Nelson, A.F. 1999, ApJ, 513, 805
- Lovelace R. V. E., Turner L., Romanova M. M., 2009, ApJ, 701, 225
- Lyra, W., Johansen, A., Zsom, A., Klahr, H., & Piskunov, N. 2009, A&A, 497, 869
- Meheut, H., Casse, F., Varnière, P., & Tagger, M. 2010, A&A, 516, A31
- Meheut, H., Keppens, R., Cassee, F., & Benz, W. 2012a, A&A, 542, A9
- Meheut, H., Yu, C., & Lai, D. 2012b, MNRAS, 422, 2399
- Meheut, H., Lovelace, R.V.E., & Lai, D. 2012c, MNRAS, in press
- Papaloizou, J. C. B., & Pringle, J. E. 1984, MNRAS, 208, 721; — 1985, MNRAS, 213, 799
- Safronov, V.S. 1960, Ann. Astrophys., 23, 982
- Sellwood, J.A. 2012, ApJ, 751, 44
- Sellwood, J.A., & Kahn, F.D. 1991, MNRAS, 250, 278
- Varnière, P., & Tagger, M. 2006, A&A, 446, L13
- Tagger, M., & Pellat, R. 1999, A&A, 349, 1003
- Tagger, M., & Varnière, P. 2006, ApJ, 652, 1457
- Tagger, M., & Melia, F. 2006, ApJL, 636, L33
- Tanga, P., Babiano, A., Dubrulle, B., & Provenzale, A. 1996, Icarus, 121, 158

Toomre, A. 1964, ApJ, 139, 1217

Umurhan, O.M. 2010, A&A, 521, A25